

**Quenching-Induced Precipitation Formation and Behavior
in Hydrous Olivine under High Pressure-Temperature
Conditions**

Ella Lubin

Advised and Read by:

Dr. Shun-ichiro Karato and Dr. Jennifer Girard

13 December, 2023

Department of Earth and Planetary Sciences, Yale University

A Senior Thesis presented to the faculty of the Department of Earth and Planetary Sciences, Yale University, in partial fulfillment of the Bachelor's Degree.

1. INTRODUCTION

The process of precipitation within Earth's interior is not well-understood. Olivine, a nominally anhydrous mineral (NAM) has often been noticed to contain hydrous precipitations. Such hydrogen inclusions have been well-observed in NAMs through experiments and spectroscopic observations, yet these past experiments focused on OH content away from the inclusion and only reported on water content from the "clean" part of the olivine samples, ignoring H₂O content from the inclusion entirely. However, depending on when and how these inclusions formed, either at high P-T or during the decrease in temperature and/or pressure, the amount of water contained in the inclusions may need to be considered. In fact, if the inclusions only formed during the process of the sample's return to room conditions (decrease in temperature or pressure), then ignoring the water content from the inclusions might lead to underestimating the amount of water capable of being dissolved within olivine under high P-T conditions. Olivine is the predominant mineral in the upper mantle, and magnesium-rich olivine is the most abundant phase, and is therefore extremely important in dictating the physical and chemical properties of that region within the earth (Bell et al., 2003). Experiments previously conducted on Mg-rich olivine have not included supersaturation (Kohlstedt, 1996), and thus the behavior of hydrogen as olivine undergoes environmental changes is unknown. Furthermore, a rock that subducts slowly and is kept at a low temperature for a long time is likely to lose most of its included hydrogen through congregated precipitation into aggregate hydrous minerals (Karato, 2006), and thus the possibility of natural hydrogen observations are eliminated. In other words, olivine samples that are collected from surface localities have experienced a broad range of thermodynamic conditions since they were at chemical equilibrium during partial melting (including cooling), a phase in which hydrogen may dissolve throughout. Thus, water loss during transportation to the surface may have occurred (Kang and Karato, 2023). These olivine rocks are believed to have a high hydrogen content while deep within Earth's interior, yet high water fugacity leads to a false report on the true quantity and behavior of hydrogen.

The solubility of hydrogen within olivine is dependent upon temperature and pressure. Zhao et al., (2004) and Kohlstedt (1996) determined the proportional temperature dependence of hydrogen solubility in olivine, and others have investigated other important factors such as pressure dependence and fugacity (Karato, 2006). Yet, the behavior of hydrogen inclusions in olivine during the cooling process have not been investigated. Hydrogen inclusions are thought

to form during cooling, when, at once high PT conditions, the temperature of olivine is reduced, forcing the hydrogen within it to form a separate phase (precipitation). This state of supersaturation is a direct result of temperature change with constant pressure. The kinetics of hydrogen precipitation in olivine due to cooling have never before been investigated in detail. We performed high-pressure, high-temperature experiments on olivine single crystals under hydrous conditions, and tested different cooling rates (quench rates) to observe the effect of the change in temperature on the formation of inclusions, and identify the origin of the inclusions.

1.1 WATER IN THE MANTLE

It has been understood for over 30 years that a large amount of water exists in the mantle (i.e: Mackwell and Kohlstedt, 1990; Kohlstedt, et al., 1996; Bell, et al., 2003) although the exact amount is still unknown. It is known that water solubility in upper mantle minerals such as olivine increases with pressure and temperature (a general increase with depth). At saturated conditions, the equivalent of 4% of the surface ocean mass of water can be hosted in the upper mantle, 20% - 100% in the transition zone, and up to 200% in the lower mantle (Ohtani, 2020). Water greatly affects the properties of minerals, such as atomic diffusivity (e.g., Costa and Chakraborty, 2008) plastic deformation (e.g., Hirth and Kohlstedt, 2003; Karato and Jung, 2003; Mei and Kohlstedt, 2000), and electrical conductivity (e.g., Wang et al., 2006; Yoshino et al., 2009). Additionally, the presence of water drastically alters the melting temperature and melt composition of the mantle peridotite system (e.g., Inoue, 1994; Kawamoto, 2004). NAMs possibly accommodate all water in the depleted mantle due to their capacity to dissolve hydrogen at condition, and provide a possible mechanism to recycle water from Earth's surface down to the deep mantle (Bell and Rossman, 1992).

Implications of Hydrous Olivine

Mackwell et al. (1985) and Karato et al. (1986) show that the strength of olivine decreases when deformed in the presence of water, which is of particular importance for mantle convection. NAMs, while not containing any hydrogen as part of their formula, are understood to often contain trace amounts of OH inconsistently placed throughout their structure as defects. The relevance of hydrogen in mantle processes depends on how much water or hydrogen can be

stored in nominally anhydrous olivine, and where it resides in the olivine lattice. Hydrogen (OH) can be considered a “point defect” in olivine (Karato, 1989; Yan, 1992; Kohlstedt, et al., 1996; Mei and Kohlstedt, 2000a), as it replaces, or substitutes for, Mg, Fe, or Si. These substitutions are not equal, due to variation in charge: twice as much hydrogen is necessary to fill a Si site than to fill a Mg or Fe site. The total solubility of hydrogen in olivine is thus expected to be coupled to the population of these point defects, while also incorporating free H₂O. When temperature is reduced (due to quenching during experiments, or, in a natural setting, due to a rock (e.g., xenolith) rising up quickly to the earth’s surface via a geological process such as volcanic eruption), OH molecules may not be as soluble in olivine as they were at high P-T, and diffuse out of the olivine crystal structure. However, depending on the rate of cooling, some OH molecules may alternatively remain trapped in the olivine in the form of inclusions which contain a hydrous phase or H₂O.

2. EXPERIMENTAL METHODS

Starting Materials

A San Carlos olivine single crystal was prepared. The single crystal was oriented along the b-direction [010]_c, using a Scanning Electron Microscope (SEM) and Electron Back Scattering Diffraction (EBSD) techniques. A cylinder was then core drilled and cut to 0.9 mm in length and 0.89-1.1 mm diameter. The single crystal was placed into a platinum capsule with length of 3-5 mm, an inner diameter of 1.6 mm, and an outer diameter of 2 mm. The capsules were loaded with a single crystal in the center, b-plane oriented lengthwise. We placed nickel foil on top and bottom of the sample to act as a protective yet penetrable surface. We used a mixture of brucite and talc powders in a 7:1 weight ratio as a source of water. This ratio ensures an excess of silicate present in the system following the dehydration reaction that occurs when the sample is placed under high P-T conditions:



The brucite-talc mixture was packed on top and bottom of the single crystal between the nickel foil and the ends of the capsule. The capsule was then welded shut (Figure 1). The capsule was loaded in the octahedral high-pressure cell.

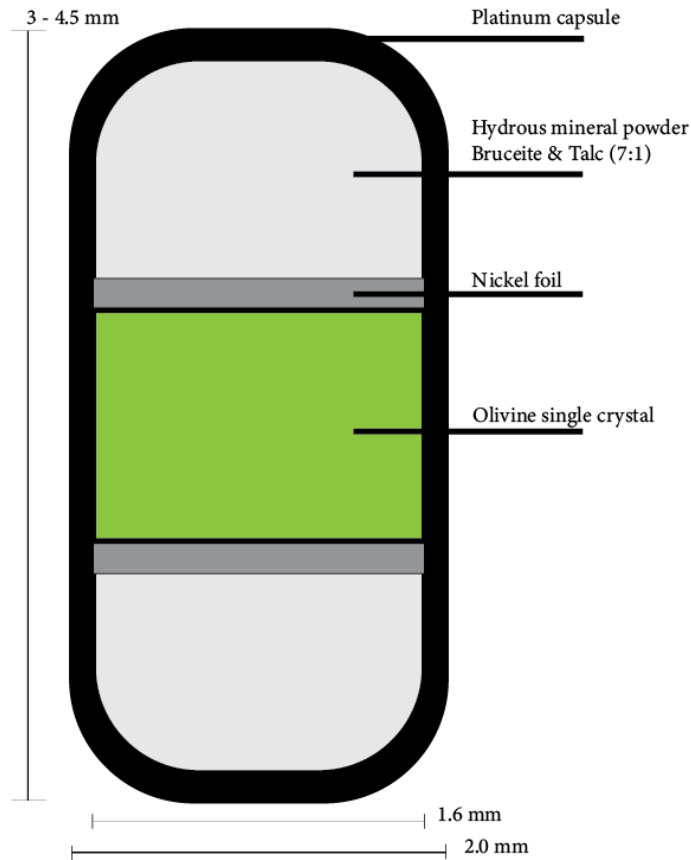


Figure 1: platinum capsule with olivine single crystal, nickel foil, and hydrous mineral powder. Not to scale

High-Pressure and High-Temperature Experiments

All experiments were conducted in a 1000-ton Kawai-type multi-anvil apparatus at Yale University. The Kawai multi-anvil press is a hydraulic press which applies pressure to the first stage anvils (6 anvils). The first stage anvils then communicate pressure to a second stage of anvils that consist of 8 tungsten-carbide cubes. Each cube has a truncated corner with a length of 17 mm, and these truncated corners are used to apply pressure on each face of the octahedra. To prevent the cubic anvils from touching when pressure is applied, each anvil is separated by gaskets made of pyrophyllite. These soft gaskets allow the production of a more hydrostatic compression.

The platinum capsules (containing the sample) were placed inside a MgO sleeve to protect the capsule from the graphite stepped furnace. The furnace was surrounded by the insulating ZrO₂ sleeve. The sleeve was placed inside the octahedra, which was surrounded by the

8 second-stage anvils. A type C thermocouple of tungsten/rhenium was inserted at the top of the cell to monitor the temperature near the capsule during the high pressure and high temperature (High P-T) experiments. The whole cell was then inserted into the Kawai press.

Compression of the sample took several hours (4-5 hrs), and the sample was kept at pressure condition (5 GPa) for several more hours before temperature was increased. Temperature increase was controlled manually through voltage-controlled resistive heating. The temperature during heating was monitored by the thermocouple near the sample. The sample was kept under high pressure and temperature conditions ~1100°C for 3.5-6.5 hours to ensure that a steady-state equilibrium was achieved within the crystal. The sample was then slowly quenched using a predetermined temperature reduction program controlled by the power supply box. The quench times and experimental P-T conditions are listed below in Figure 2. Note: K2217 has a listed quench time of 0 minutes. This is the approximate length of time it took for the sample to quench from condition to room temperature once the heating power supply was turned off, as opposed to applying a predetermined temperature reduction program.

SAMPLE	PRESSURE (GPa)	TEMPERATURE (°C)	TIME QUENCHED (Mins)	THICKNESS AFTER QUENCH (Microns)
K2215	5	1100	20	270
K2217	5	1100	0	100
K2222	5	1100	40	680
K2226	5	1100	40	230

Figure 2: Experimental Conditions

After decompression, the cell was removed from the anvils, and the sample was extracted from the capsule. To monitor for saturation, the capsules were dismembered under water through the lens of a microscope. This protocol ensured that, upon capsule puncture, any escaping bubbles could be seen. Bubbles are evidence of sample saturation (excess of water) and indicate the transformation of the H from the hydrous mineral powder into a fluid.

Fourier Transform Infrared Spectroscopy

Fourier transform infrared (FTIR) spectroscopy is the most commonly applied tool for measuring such low hydrogen concentrations as are observed in olivine. FTIR works by shining a beam of IR radiation of different wavelengths through a user-designated point on the sample. Some of the radiation is absorbed by the sample and the rest is transmitted through. The absorbed radiation causes the covalent bonds within molecules to excite and vibrate, acting as a spring. Each known molecule absorbs IR radiation at a different frequency dependent upon their atomic and bond composition, thus producing a unique molecular “fingerprint” of vibrational frequencies. FTIR spectroscopy works differently from regular IR spectroscopy by providing higher wavelength accuracy through the initial representation of absorbance as a function of mirror position (from which the source energy is originally transmitted to) instead of wavelength.

A beam aperture of 25-50 μm was used for the analyses. Raw spectra produced by the FT function were adjusted with a baseline correction, and normalized with consideration of thickness. Each spectrum was extracted and corrected. Presence of OH/H₂O absorption in the sample is indicated by peaks or curves in the wavenumber region between 3000-4000 cm^{-1} on the FTIR. We used the integration of this region to calculate H₂O and OH content in each sample.

3. RESULTS

OH and H₂O content, listed in Figure 3, were calculated from thickness-corrected FTIR spectra using Eq. 1 from Paterson (1982).

$$c_{OH} = \int \frac{K(\bar{\nu})}{150\gamma(3780-\bar{\nu})} d(\bar{\nu}) \quad (1)$$

where c_{OH} is the molar hydroxyl concentration, γ is the orientation factor, $K(\bar{\nu})$ is the absorption coefficient (in mm^{-1}) at wavenumber $\bar{\nu}$, and $d(\bar{\nu})$ is the difference between sequential wavenumbers. For unpolarized radiation, with the O-H bond direction in the same plane as the electric vector of the infrared radiation, $\gamma = 0.5$. H₂O content is calculated as shown in Eq. 2, where c_{H_2O} is the molar H₂O concentration, c_{OH} is the molar hydroxyl concentration.

$$c_{H_2O} = \frac{c_{OH}}{16.3} \quad (2)$$

K2217	H2O (ppm [wt])	OH (H/10 ⁶ Si)	K2215	H2O (ppm [wt])	OH (H/10 ⁶ Si)	K2222	H2O (ppm [wt])	OH (H/10 ⁶ Si)	K2226	H2O (ppm [wt])	OH (H/10 ⁶ Si)
Radial			Radial			Radial			Radial		
0	45.9684	749.285	0	528.9209	8621.411	0	20.9572	341.602	0	108.562	1769.56
1	197.933	3226.32	1	551.35	8987	1	84.605	1379.06	1	127.913	2084.98
2	175.012	2852.69	2	548.894	8946.97	2	80.8784	1318.32	2	89.298	1455.56
3	236.148	3849.2	3	495.901	8083.19	3	40.7366	664.006	3	120.534	1964.7
4	248.272	4046.83	4	458.028	7465.86	4	26.8827	436.188	4	125.201	2040.78
5	171.107	2789.05	5	627.426	10227	5	22.0942	360.136	5	60.0884	979.441
6	198.317	3232.56	6	556.972	9078.64	6	21.6629	353.105	6	105.978	1727.45
7	572.468	9331.23	7	531.008	8655.44	7	28.6669	467.27	7	123.589	2014.49
8	368.873	6012.63				8	48.2005	785.668	8	140.629	2292.25
9	587.947	9581.91				9	30.4272	495.964	9	55.6111	906.46
10	235.302	3835.42	Random						10	56.1098	914.59
11	31.229	509.033	0	431.732	7037.24	Random			Random		
12	242.568	3953.86	1	610.684	9954.16	0	61.6582	1005.03	0	148.587	2421.97
13	7.28589	118.76	2	400.106	6521.72	1	63.4075	1033.54	1	102.401	1669.14
14	23.8114	388.125	3	548.743	8944.51	2	44.5328	725.885	2	121.179	1975.21
15	92.1896	1502.69	4	508.924	8295.45	3	41.3663	674.27	3	141.058	2299.24
16	304.674	4966.18	5	626.829	10217.3	4	31.4231	512.197	4	222.412	3625.32
Random			6	510.795	8325.96	5	28.9975	472.66	5	115.892	1889.04
0	52.7947	860.553	7	571.937	9322.58	6	29.0239	473.089	6	73.1401	1192.18
2	31.841	519.009				7	157.541	2567.92	7	85.3668	1391.48
3	167.849	2735.94				8	198.815	3240.68	8	155.428	2533.48
6	424.566	6920.42							9	4754.81	77503.4
7	108.446	1767.68									
8	239.489	3903.67									

Figure 3: H₂O and OH content calculated from eq. 1 and eq. 2. K2217: 0 minute quench; K2215: 20 minute quench; K2222 & K2226: 40 minute quench. For all radial mapping, point 0 is the farthest exterior point on the crystal while the highest number listed for each sample is the center of the crystal.

Radial mapping, seen in Figure 4, was completed using linear positioning on FTIR. Radial mapping was done in hopes of examining the comparative spatial distributions of hydrogen throughout the samples. Random mapping (Figure 5) was completed using subjective, user-selected points on particularly noticeable features (i.e.: an extremely dark inclusion, a region void of marks, a region which contains light inclusions, etc.). Random map points were analyzed through the Java based image processing program ImageJ/Fiji to assess the relationship between H₂O/OH content and pixel grayscale, shown in Figure 6. Grayscale is measured with values between 0-255, 0 being completely black and 255 completely white. Images were initially converted into BW from RGB to perform precise analysis.

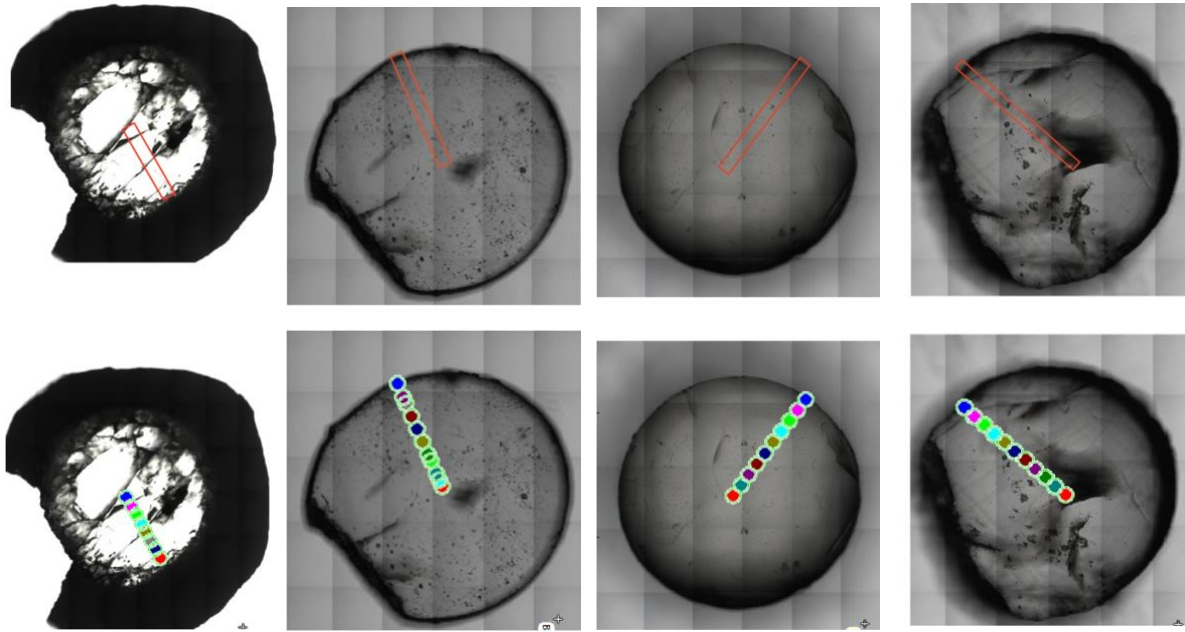


Figure 4: Radial map points (below) and the features they cover (above). From left to right: K2215 (20 minute quench), K2217 (0 minute quench), K2222 (40 minute quench), K2226 (40 min quench).

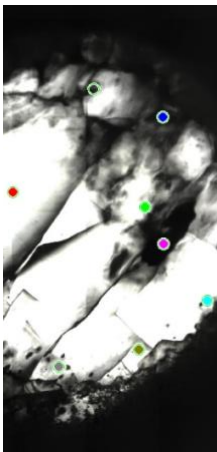


Figure 5: Random map points. From left to right: K2215 (20 minute quench), K2217 (0 minute quench), K2222 (40 minute quench), K2226 (40 min quench).

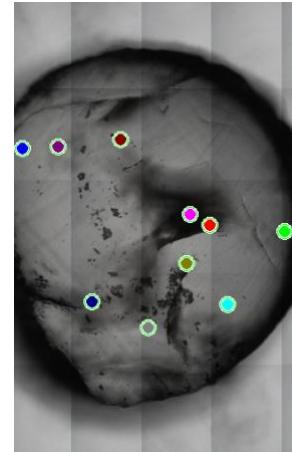
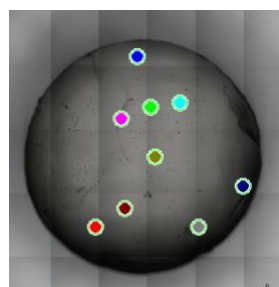
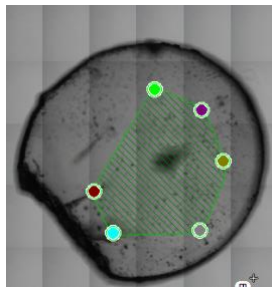
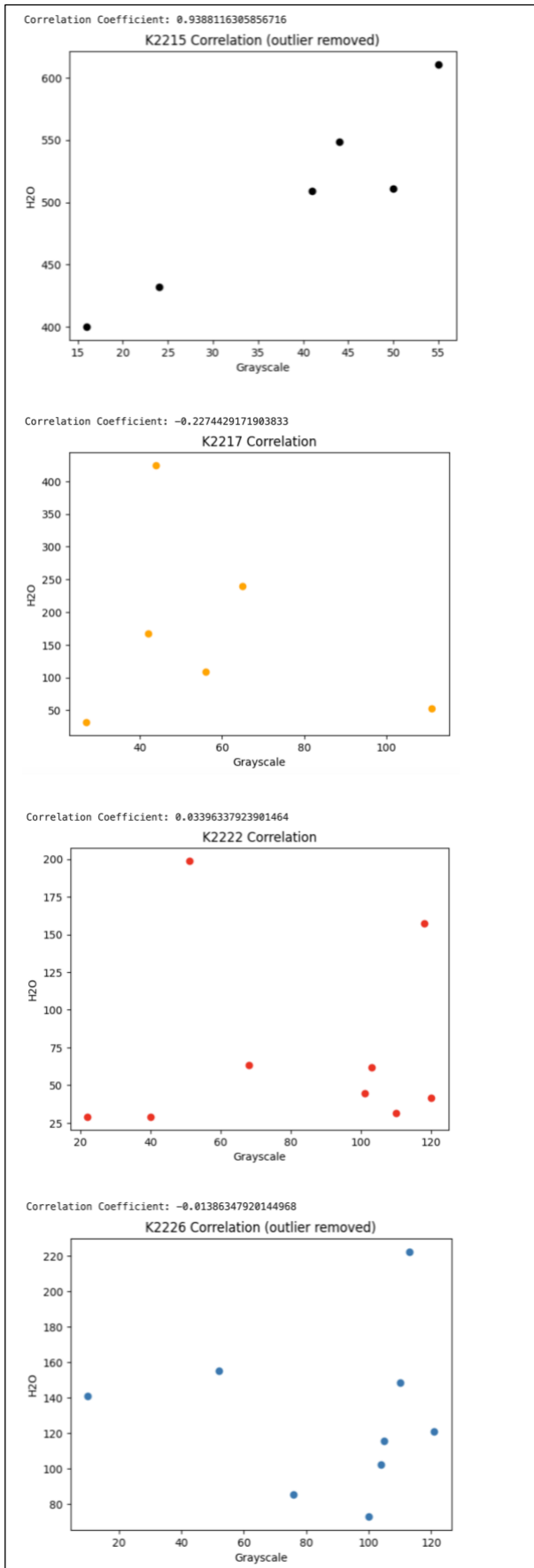


Figure 6: Grayscale value to H₂O correlation (H₂O content in ppm wt, grayscale intensity 0-255).



In order to assess and compare the radial map points, each sample was plotted by water content. The quantity of radial map points varied by sample, so the point locations were normalized between 0 and 1. Figure 7 illustrates the saturation curve as a function of pressure at 1100°C (Kohlstedt et al., 1996). All samples were brought to 5 GPa, which corresponds to a water concentration of +/- 500 ppm wt. Figure 8 shows no evident distributional pattern, but does illustrate a clear lack of full saturation in the two samples quenched for 40 minutes (K2222 and K2226), as H₂O concentrations are far below expected saturation levels.

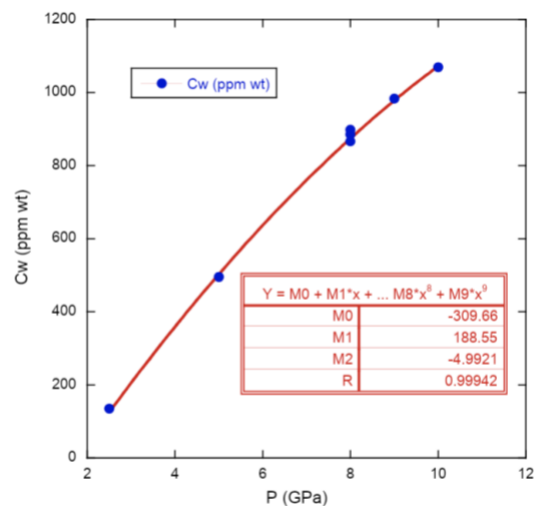


Figure 7: water concentration (H₂O) in ppm wt as a function of pressure (GPa) at 1100°C.

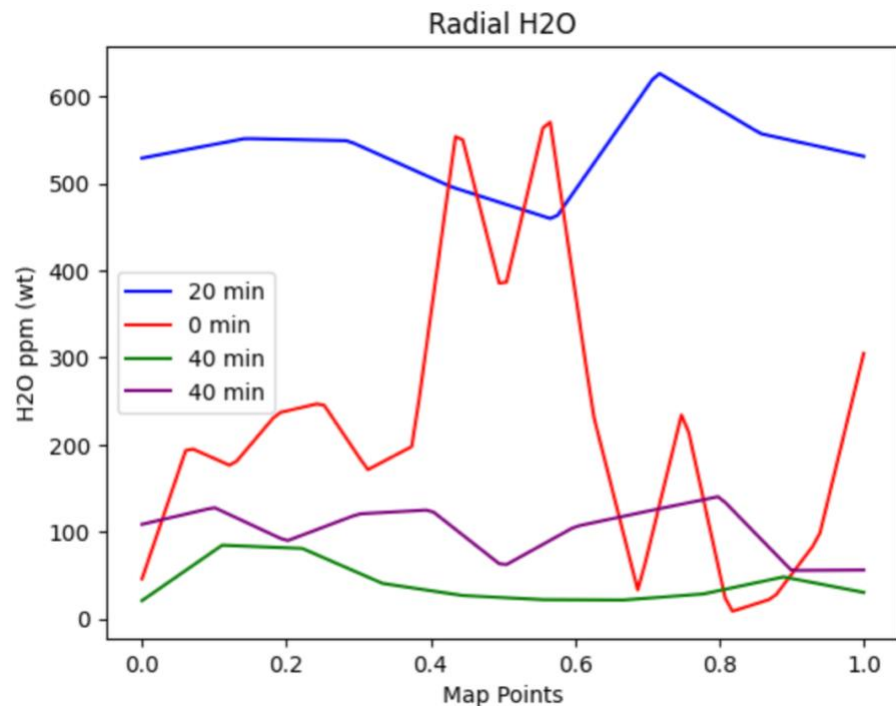


Figure 8: Spatial distribution of H₂O through radial FTIR map points. Point 0 is the exterior of the crystal, point 1 is the center of the crystal. The two samples quenched for 40 minutes show H₂O levels far below expected levels of a fully saturated sample.

Structure-bonded OH and free H₂O

Extracted FTIR spectra corrected for thickness display several distinct shapes which reveal composition and distinguish between different forms of hydrogen within the sample. Spectra are graphed by absorption coefficient as a function of wavenumber. Absorption coefficient refers to the quantity of radiation absorbed by a material of a given thickness. Wavenumber is the number of waves in a given distance, directly inverse to wavelength. Presence of structure-bonded OH is evidenced by one or multiple sharp peaks in the 3,000-4,000 wavenumber range (ex: Figure 9a). Comparatively, free H₂O exists as a liquid or amorphous fluid in the structure, whose vibrational frequencies overlap and cover a wide range, producing a broad curve in the graph. Figure 10 is an example of such curves, found in K2217 (0 minute quench). Although the absorption coefficient is much lower than in Fig. 9a, the curve still maintains as evidence for free H₂O. In comparison, Fig. 9b is an example of negligible H content; K2226 (40 minute quench) did not reach a state of saturation at condition or lost its hydrogen during quench, and all of the spectra from the sample illustrate “noise” and insignificant levels of hydrogen (Note: wavenumber range is in descending order on Fig. 9a and 9b, and ascending order on Fig. 10).

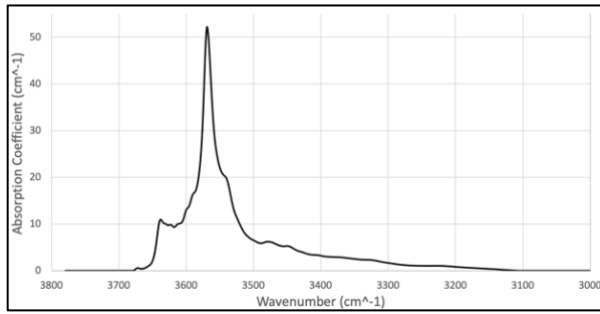


Figure 9: FTIR corrected spectra extracted from K2215 (20 minute quench). A sharp peak and high absorption coefficient are evidence of a high quantity of structure-bonded OH.

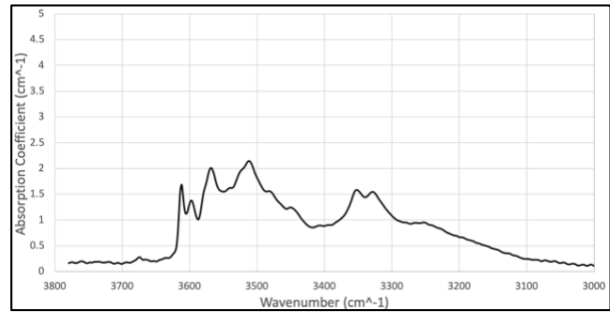


Figure 9b: FTIR corrected spectra extracted from K2226 (40 minute quench). No distinct sharp peak or broad curve. Very low absorption coefficients. Graphical pattern is common with background noise from the FTIR, debris left on the sample from the experiment, or insignificant levels of hydrogen.

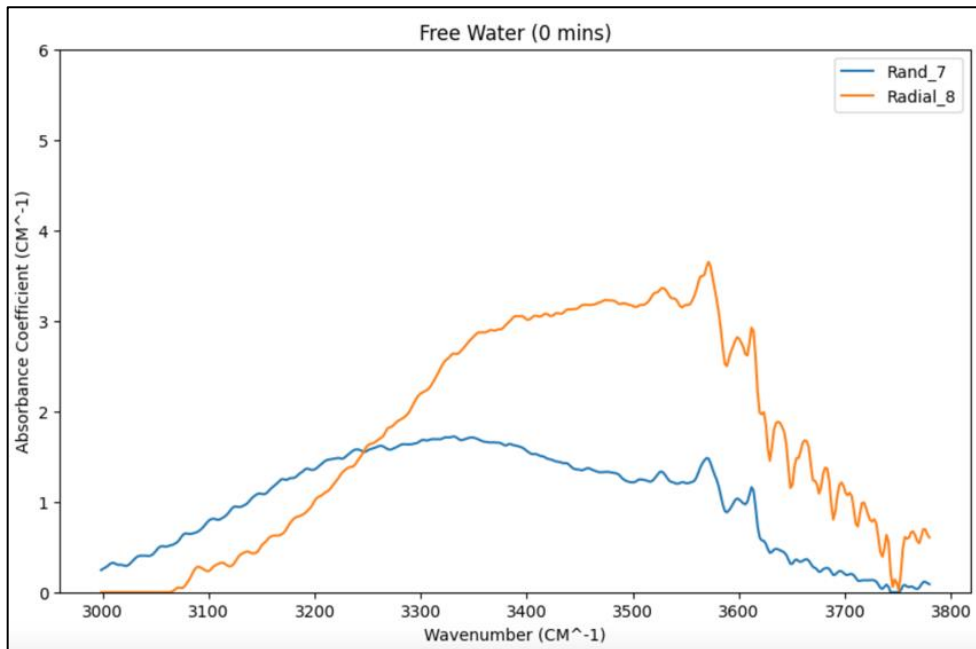


Figure 10: Two extracted FTIR corrected spectra from K2217 (0 minute quench). Broad curves are evidence of free H₂O (not bound in the crystal structure), even with such low absorption coefficients.

Absorption is independent of location, which confirms a near chemical equilibrium (achievement is attempted by leaving the sample in condition for several hours before quenching), shown by Figure 11.

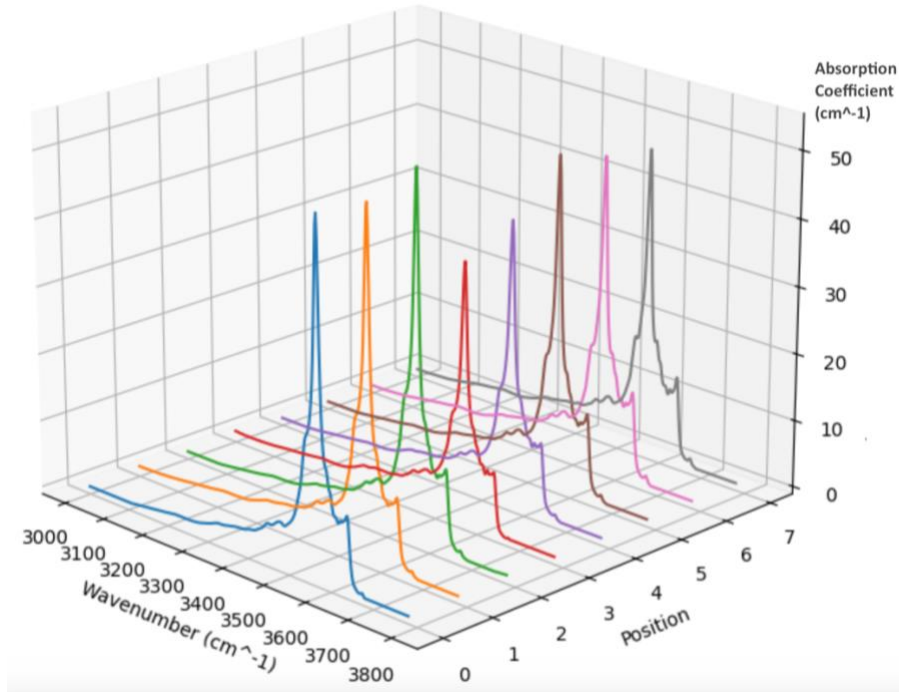


Figure 11: Absorption coefficient as a function of wavenumber, compared by radial position (0 as exterior, 7 as radial center) for K2215 (20 minute quench). There is no clear spatial distributional pattern, which illustrates near chemical equilibrium while at condition.

Additionally, absorption coefficient of a spectra is an indicator of H solubility within the sample. Higher OH concentrations produce higher coefficients. Figure 12 illustrates this concept, when compared to Fig. 3. K2217 (0 minute quench) produced only 3 map points with an absorption coefficient above 2.5 cm^{-1} , and only 6 map points with an OH concentration above 4000 cm^{-1} .

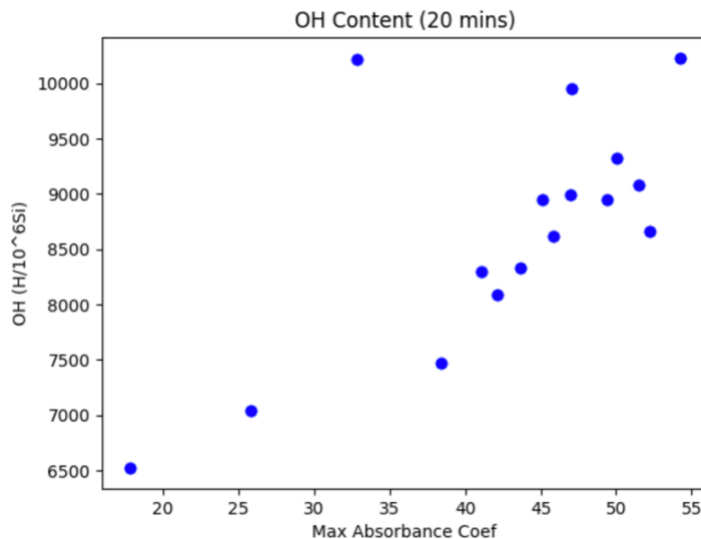


Figure 12: The relationship between OH concentration and maximum absorption coefficient appears to be quite strong in K2215 (20 minute quench).

4. DISCUSSIONS

The results shown in Fig. 3, Fig. 8, and Fig. 12 can be used to infer a temporal relationship between quench time and OH/H₂O content in hydrous olivine. K2215 (20 minute quench) exhibits much higher concentrations of OH/ H₂O than K2217 (0 minute quench), corroborated by higher absorption coefficients overall. Furthermore, while K2222 and K2226 (40 minute quench) did not show levels equivalent to full saturation, a previous identical experiment in the Karato lab with a quench time of 60 minutes resulted in a shattered crystal (presumably from hydrogen precipitations growing too large for the olivine crystal to support at a less malleable state of decreased temperature), supporting the temporal relationship realized in these experiments. While there is no evident spatial pattern of H distribution throughout the samples, this may prove total or near chemical equilibrium while at condition. According to previous studies on hydrogen diffusion in olivine, the hydrogen in our experiments had enough time to diffuse throughout the whole crystal after 3-6 hours in high P-T conditions for the size of the olivine single crystal that we used (~1 mm in diameter and 100-700 μm thick). Moreover, the high levels of OH/ H₂O measured provide insight into the correct site substitution (Mg or Si), as more OH is required to fill Si sites. These point defects alter the crystal fabric, affect the flow geometry, and influence the seismic anisotropy of the upper mantle (Jung and Karato, 2001).

These relationships highlight the natural phenomenon of hydrous olivine in the mantle and its behaviors. Mantle convection is driven in part by the strength and deformation of predominant minerals. Olivine, as previously discussed in sections 1 and 1.1, is the predominant mineral in the upper mantle. The strength of olivine is affected by the presence of water, and olivine will creep five times faster under hydrous conditions (Mei and Kohlstedt, 2000a). Mantle viscosity, a driving and resulting factor of mantle convection, vary depending on the geochemical environment, which dictates how hydrated upper mantle olivine will become (Bolfan-Casanova, 2005). The water flux between the surface oceans and the mantle is also controlled by mantle convection. For example, the water flux returned to the mantle by subducting slabs is $\sim 8.7 \times 10^{11}$ kg/year, while the amount of water degassed to the surface (through magmatism) is 2×10^{11} kg/year (Ohtani, 2020). That leaves 6.7×10^{11} kg/year of water unaccounted for. Some researchers have estimated that water penetrating down into the transition zone and lower mantle, while others estimate it is recycled throughout the upper mantle. These

uncertainties highlight the importance of specifying and understanding water reservoirs, such as olivine.

Insights on Solubility

The inclusion of free water, H₂O not bonded within the crystal structure, as shown in Fig. 10 is evidence of more hydrogen held within the sample than previous experiments documented. Hydrogen solubility within olivine may be calculated using Eq. 3 by Kang & Karato (2023).

$$C_{OH} = A \cdot f_{H_2O}^n \cdot \exp\left(-\frac{\Delta E + P\Delta V}{RT}\right) \quad (3)$$

Where C_{OH} is the hydrogen content in a mineral, A is a constant which essentially contains the entropy of reaction, $f_{H_2O}^n$ is the fugacity of water, n is an exponent that depends on the mechanisms of water dissolution, ΔE and ΔV are the reaction energy and the volume change of the solids after the dissolution of hydrogen respectively, R is the gas constant, T is the temperature (in K) and P is pressure.

The study of the solubility of hydrogen within olivine provides a better understanding of water behavior in the mantle, and may allow a more accurate calculation of water concentrations below investigable depths of the upper mantle. Net water solubility in olivine increases with depth (Kang and Karato, 2023), although any insights made about solubility below the pressure limits of these experiments (5 GPa ~ 120 km depth) will be extrapolations. This study did not examine the factor of oxygen fugacity and its influence on solubility, however, fugacity most definitely affects the aspects discussed above (temperature and time dependence, and OH substitution sites). Fugacity may be difficult to accurately measure and control in high pressure-temperature experiments such as these due to the variation between experimental (ideal) conditions and natural conditions: a sample is saturated or supersaturated in the laboratory, yet is most likely often under-saturated in its natural environment.

Discussion on experimental methods and further study

The high PT experiments and IR analysis that were completed for this thesis may be improved and extended for continued study of this topic. Further examination of inclusions using Transmission Electron Microscope (TEM) will give insight into the content inside the inclusions

and will indicate whether they include serpentinized olivine (hydrous olivine), olivine transformed to another pressure phase, free H₂O, or hydrous minerals. Additionally, intensive and more thorough IR mapping will clarify the spatial pattern of OH directly surrounding the inclusions. If TEM measurements report hydrous olivine within the inclusions, then we expect that the regions directly surrounding them will be drier as a result. Future research that builds on the conclusions of this paper should be the investigation of transient creep in wet conditions, and the possible role which hydrous olivine played in the origin of life on Earth.

ACKNOWLEDGMENTS

I would like to thank my advisor, Dr. Shun-ichiro Karato, for his patience and helpful instruction, and Dr. Jennifer Girard for her endless guidance, vast expertise, and inexhaustible support throughout the duration of this project. I entered this project with no prior lab experience, and Jennifer taught me the process and protocol of every single step, from cutting single crystals to troubleshooting FTIR data collection issues. I am also grateful to Quinting Jiang for her mentorship in the laboratory. Thank you to DUS Mary-Louise Timmermans and DUS Celli Hull for their encouragement and advice throughout my time at Yale. Lastly, I would like to extend my gratitude to all the EPS professors whom I have taken courses from, graduate mentors, and undergraduate peers: Thank you for helping me grow as a scientist and broadening my understanding of, and curiosity for, the physical world we live in.

REFERENCES

- Bai, Q., & Kohlstedt, D. L. (1988). Substantial hydrogen solubility in olivine and implications for water storage in the mantle. In *Honja, S. J. Mar. Res* (Vol. 33, Issue 9).
- Bell, D. R., & Rossman, G. R. (1992). Water in Earth's Mantle: The Role of Nominally Anhydrous Minerals. In *Science*. <https://www.science.org>
- Bell, D. R., Rossman, G. R., Maldener, J., Endisch, D., & Rauch, F. (2003). Hydroxide in olivine: A quantitative determination of the absolute amount and calibration of the IR spectrum. *Journal of Geophysical Research: Solid Earth*, 108(B2). <https://doi.org/10.1029/2001jb000679>
- Bolfan-Casanova, N. (2005). Water in Earth's mantle. *The Mineralogical Society*.
- Costa, F., & Chakraborty, S. (2008). The effect of water on Si and O diffusion rates in olivine and implications for transport properties and processes in the upper mantle. *Physics of the Earth and Planetary Interiors*, 166(1–2), 11–29. <https://doi.org/10.1016/j.pepi.2007.10.006>
- Hirth, G., & Kohlstedt, D. (2004). Rheology of the upper mantle and the mantle wedge: A view from the experimentalists. In *Geophysical Monograph Series* (Vol. 138, pp. 83–105). Blackwell Publishing Ltd. <https://doi.org/10.1029/138GM06>
- Inoue, T. (1994). Effect of water on melting phase relations and melt composition in the system Mg₂SiO₄-MgSiO₃-H₂O up to 15 GPa. In *Physics of the Earth and Planetary Interiors* (Vol. 85).
- Jung, H., & Karato, S.-I. (2001). Water-Induced Fabric Transitions in Olivine. In *Science Magazine* (Vol 293). <https://www.science.org>
- Kang, L., & Karato, S. ichiro. (2023). Hydrogen Partitioning Between Olivine and Orthopyroxene: Implications for the Lithosphere-Asthenosphere Structure. *Journal of Geophysical Research: Solid Earth*, 128(2). <https://doi.org/10.1029/2022JB025259>
- Karato, S. (1989). Grain growth kinetics in olivine aggregates. In *Tectonophysics* (Vol. 168).
- Karato, S. I. (2018). Remote sensing of hydrogen in Earth's mantle. In *Water in Nominally Anhydrous Minerals* (pp. 343–376). Walter de Gruyter GmbH. <https://doi.org/10.2138/rmg.2006.62.15>
- Karato, S. I., & Jung, H. (2003). Effects of pressure on high-temperature dislocation creep in olivine. *Philosophical Magazine*, 83(3), 401–414. <https://doi.org/10.1080/0141861021000025829>

- Karato, S., Paterson, M. S., & FitzGerald, J. D. (1986). Rheology of synthetic olivine aggregates: Influence of grain size and water. *Journal of Geophysical Research: Solid Earth*, 91(B8), 8151–8176. <https://doi.org/10.1029/jb091ib08p08151>
- Karato, S.-I. (2006). Influence of Hydrogen-Related Defects on the Electrical Conductivity and Plastic Deformation of Mantle Minerals: A Critical Review. In *Geophysical Monograph Series* (Vol. 168, pp. 131–145). Blackwell Publishing Ltd. <https://doi.org/10.1029/168GM09>
- Kawamoto, T. (2004). Hydrous phase stability and partial melt chemistry in H₂O-saturated KLB-1 peridotite up to the uppermost lower mantle conditions. *Physics of the Earth and Planetary Interiors*, 143(1–2), 387–395. <https://doi.org/10.1016/j.pepi.2003.06.003>
- Kohlstedt, D. L., Keppeler, H., & Rubie, D. C. (1996). Solubility of water in the a, b and g phases of (Mg,Fe)₂SiO₄. In *Contrib Mineral Petrol* (Vol. 123). Springer-Verlag.
- Mackwell, S. J., & Kohlstedt, D. L. (1990). Diffusion of hydrogen in olivine: implications for water in the mantle. *Journal of Geophysical Research*, 95(B4), 5079–5088. <https://doi.org/10.1029/JB095iB04p05079>
- Mackwell, S. J., Kohlstedt, D. L., & Paterson, M. S. (1985). The role of water in the deformation of olivine single crystals. *Journal of Geophysical Research*, 90(B13). <https://doi.org/10.1029/jb090ib13p11319>
- Martin, R. F., & Donnay, G. (1972). Hydroxyl in the Mantle. In *American Mineralogist* (Vol. 57). http://pubs.geoscienceworld.org/msa/ammin/article-pdf/57/3-4_Part_1/554/4256370/am-1972-554.pdf
- Mei, S., & Kohlstedt, D. L. (2000a). Influence of water on plastic deformation of olivine aggregates 1. Diffusion creep regime. *Journal of Geophysical Research: Solid Earth*, 105(B9), 21457–21469. <https://doi.org/10.1029/2000jb900179>
- Mosenfelder, J. L., Deligne, N. I., Asimow, P. D., & Rossman, G. R. (2006). Hydrogen incorporation in olivine from 2-12 GPa. *American Mineralogist*, 91(2–3), 285–294. <https://doi.org/10.2138/am.2006.1943>
- Mosenfelder, J. L., Voyer, M. Le, Rossman, G. R., Guan, Y., Bel, D. R., Asimow, P. D., & Eiler, J. M. (2011). Analysis of hydrogen in olivine by SIMS: Evaluation of standards and protocol. *American Mineralogist*, 96(11–12), 1725–1741. <https://doi.org/10.2138/am.2011.3810>

- Ohtani, E. (2020). The role of water in Earth's mantle. *National Science Review*, (Vol. 7, issue 1), 224-232. <https://doi.org/10.1093/nsr/nwz071>
- Otsuka, K., & Karato, S. ichiro. (2011). Control of the water fugacity at high pressures and temperatures: Applications to the incorporation mechanisms of water in olivine. *Physics of the Earth and Planetary Interiors*, 189(1-2), 27-33. <https://doi.org/10.1016/j.pepi.2011.09.007>
- Paterson, M. S. (1982). The determination of hydroxyl by infrared adsorption in quartz, silicate glasses and similar materials. *Bulletin de Mineralogie*, 105(1), 20-29. <https://doi.org/10.3406/bulmi.1982.7582>
- Ritterbex, S., Carrez, P., & Cordier, P. (2020). Deformation across the mantle transition zone: A theoretical mineral physics view. *Earth and Planetary Science Letters*, 547. <https://doi.org/10.1016/j.epsl.2020.116438>
- Wang, D., Mookherjee, M., Xu, Y., & Karato, S. (2006). *The effect of water on the electrical conductivity of olivine*.
- Yoshino, T., Matsuzaki, T., Shatskiy, A., & Katsura, T. (2009). The effect of water on the electrical conductivity of olivine aggregates and its implications for the electrical structure of the upper mantle. *Earth and Planetary Science Letters*, 288(1-2), 291-300. <https://doi.org/10.1016/j.epsl.2009.09.032>
- Zhao, Y. H., Ginsberg, S. B., & Kohlstedt, D. L. (2004). Solubility of hydrogen in olivine: Dependence on temperature and iron content. *Contributions to Mineralogy and Petrology*, 147(2), 155-161. <https://doi.org/10.1007/s00410-003-0524-4>